ACES Asian Chemical Editorial Society

DOI: 10.1002/asia.201900634

CHEMISTRY AN ASIAN JOURNAL Full Paper

Special Issue

MIL-53(Al) as a Versatile Platform for Ionic-Liquid/MOF Composites to Enhance CO_2 Selectivity over CH_4 and N_2

Safiyye Kavak[+],[a, c] H. Mert Polat[+],[a, c] Harun Kulak[+],[b, c] Seda Keskin,*[b, c] and Alper Uzun*[b, c, d]

Abstract: Five different imidazolium-based ionic liquids (ILs) were incorporated into a metal–organic framework (MOF), MIL-53(Al), to investigate the effect of IL incorporation on the CO_2 separation performance of MIL-53(Al). CO_2, CH_4, and N_2 adsorption isotherms of the IL/MIL-53(Al) composites and pristine MIL-53(Al) were measured to evaluate the effect of the ILs on the CO_2/CH_4 and CO_2/N_2 selectivities of the MOF. Of the composite materials that were tested, [BMIM][PF_6]/MIL-53(Al) exhibited the largest increase in CO_2/CH_4 selectivity, 2.8-times higher than that of pristine MIL-53(Al), whilst [BMIM][$MeSO_4$]/MIL-53(Al) exhibited the largest increase in CO_2/N_2 selectivity, 3.3-times higher than that of pristine MIL-53(Al). A comparison of the CO_2 separation potentials of the IL/MOF composites showed that the [BMIM][BF_4]- and [BMIM][PF_6]-incorporated MIL-53(Al) composites both showed enhanced CO_2/N_2 and CO_2/CH_4 selectivities at pressures of 1–5 bar compared to composites of CuBTC and ZIF-8 with the same ILs. These results demonstrate that MIL-53(Al) is a versatile platform for IL/MOF composites and could help to guide the rational design of new composites for target gas-separation applications.

1. Introduction

Metal–organic frameworks (MOFs) are porous solids with high surface areas, permanent porosities, good thermal and chemical stabilities, and customizable chemistry and functionality.[1,2] Because of these excellent properties, MOFs have been studied in a large variety of fields, such as catalysis,[3] luminescence science,[4] medical applications,[5] membrane technology,[6,7] and gas storage, separation, and purification.[8] Among these applications, MOFs have received significant interest for CO_2 capture and separation, and are thought to be efficient and promising materials in this field.[9,10]

MOFs can be synthesized from a wide variety of metal ions and organic linkers, and their chemical and physical properties can be tuned by using postsynthetic modification methods.[11] Several studies have reported that the gas-adsorption affinity and selectivity of MOFs can be enhanced by incorporating functional groups, such as sulfonic acids and amines, into the pores through ligand modification.[12,13] In this respect, a relatively recent approach was developed, in which MOFs were combined with ionic liquids (ILs), which are molten salts of organic or inorganic anions and cations.[14] Theoretically, an infinite number of ILs can be synthesized by combining different pairs of anions and cations. Such a high number of structural possibilities offers significant opportunities to tailor the IL structure for exceptional performance in any desired field.[15,16] For example, if an IL exhibits opposite affinities for two different gas molecules, it could be an excellent material for the separation of these gases.[17] Moreover, ILs also possess other useful properties, such as inflammability, negligible volatility, and relatively high chemical and thermal stabilities,[18] in addition to being an ideal medium for the synthesis of MOFs.[19] They have been studied as lubricants,[20] electroelastic materi-

[a] S. Kavak,[+] H. M. Polat[+]
Department of Materials Science and Engineering
Koç University
Rumelifeneri Yolu, 34450 Sariyer
Istanbul (Turkey)

[b] H. Kulak,[+] Prof. S. Keskin, Prof. A. Uzun
Department of Chemical and Biological Engineering
Koç University
Rumelifeneri Yolu, 34450 Sariyer
Istanbul (Turkey)
E-mail: skeskin@ku.edu.tr
auzun@ku.edu.tr

[c] S. Kavak,[+] H. M. Polat,[+] H. Kulak,[+] Prof. S. Keskin, Prof. A. Uzun
Koç University TÜPRAŞ Energy Center (KUTEM)
Koç University
Rumelifeneri Yolu, 34450 Sariyer
Istanbul (Turkey)

[d] Prof. A. Uzun
Koç University Surface Science and Technology Center (KUYTAM)
Koç University
Rumelifeneri Yolu, 34450 Sariyer
Istanbul (Turkey)

[+] These authors contributed equally in this work.

Supporting information and the ORCID identification number(s) for the author(s) of this article can be found under: https://doi.org/10.1002/asia.201900634.

Special Issue This manuscript is part of a special issue on Metal-Organic Frameworks and Their Applications. Click here to see the Table of Contents of the special issue.

als,[21] fuel-cell electrolytes,[22] solvents and catalysts,[23] and adsorbents.[24] Because of the outstanding properties of MOFs and ILs, the postsynthetic modification of MOFs with ILs holds great potential for improving the performance of the parent MOFs in a range of applications, especially in gas separation.[25]

Several recent studies have reported the synthesis of IL/MOF composites and tested them for gas separation. For example, we investigated the incorporation of 1-*n*-butyl-3-methylimidazolium tetrafluoroborate ([BMIM][BF_4]) into copper benzene-1,3,5-tricarboxylate (CuBTC; also known as HKUST-1, Hong Kong University of Science and Technology), and reported an increase in the selectivity of the MOF for CH_4 over CO_2, N_2, and H_2.[26] Two ILs, 1-*n*-butyl-3-methylimidazolium hexafluorophosphate ([BMIM][PF_6]) and 1-*n*-butyl-2,3-dimethylimidazolium hexafluorophosphate ([BMMIM][PF_6]), were also incorporated into CuBTC, and the selectivity of the MOF for both CO_2/N_2 and CH_4/N_2 was shown to be improved.[27] Furthermore, the incorporation of [BMIM][BF_4], [BMIM][PF_6], and 1-*n*-butyl-3-methylimidazolium thiocyanate ([BMIM][SCN]) into zinc 2-methylimidazolate (ZIF-8; ZIF stands for zeolitic imidazolate framework) led to enhanced CO_2 selectivity over CH_4 and N_2.[28–30] Mohamedali et al. impregnated 1-*n*-butyl-3-methylimidazolium acetate ([BMIM][OAc]) and 1-ethyl-3-methylimidazolium acetate ([EMIM][OAc]) into ZIF-8 to improve its CO_2/N_2 selectivity.[31] In a different approach, 1-(2-hydroxyethyl)-3-methylimidazolium dicyanamide ([HEMIM][DCA]) was deposited onto the external surface of ZIF-8 to enhance its CO_2/CH_4 selectivity.[32] As presented above, almost all of the gas-adsorption and gas-separation studies on IL/MOF composites reported to date have focused on one type of MOF, typically CuBTC or ZIF-8, and only a few types of ILs. However, experimental investigation of the incorporation of ILs with different physical and chemical properties into MOFs with different textural and chemical properties would play an important role in improving our understanding of the interactions between ILs and MOFs, which would help to guide the rational design of new IL/MOF composites with improved gas-separation performance. Very recently, we extended this approach to synthesize a MOF that has not previously been considered for IL/MOF composites, that is, aluminum 1,4-benzenedicarboxylate (MIL-53(Al); MIL = Matériaux de l'Institut Lavoisier).[33] We postsynthetically modified MIL-53(Al) by incorporating 1-*n*-butyl-3-methylimidazolium methyl sulfate ([BMIM][$MeSO_4$]), which led to a significant enhancement in the CO_2 separation performance of the composite compared to the pristine MOF. These results demonstrated the high potential of MIL-53(Al) for this approach.

Motivated by these preliminary results on MIL-53(Al) composites, herein, we report the incorporation of a family of ILs that comprised the same cation (1-*n*-butyl-3-methylimidazolium, $[BMIM]^+$) but different types of anion (tetrafluoroborate, $[BF_4]^-$; hexafluorophosphate, $[PF_6]^-$; trifluoromethanesulfonate, $[CF_3SO_3]^-$; hexafluoroantimonate, $[SbF_6]^-$; and bis(trifluoromethanesulfonyl)amide, $[NTf_2]^-$) into this MOF. The new IL/MOF composites were characterized by using a range of experimental techniques. Then, we analyzed the CO_2, CH_4, and N_2 adsorption performance of these composites to assess their CO_2/CH_4 and CO_2/N_2 selectivities. We also compared the CO_2/CH_4 and CO_2/N_2 selectivities of composites of [BMIM][BF_4] and [BMIM][PF_6] with MIL-53(Al), CuBTC,[26,27], and ZIF-8[28,29] to understand the effect of the physical and chemical properties of ILs and MOFs on their gas-separation performance. Furthermore, we also provided a comprehensive comparison of the CO_2/CH_4 and CO_2/N_2 selectivities of IL/MIL-53(Al) composites with some pristine MOFs. The results presented in this work will provide new insight into the fundamental principles for selecting the best IL and MOF couples for the design and development of new IL/MOF composites with high CO_2 separation performance.

2. Results and Discussion

Herein, we report the characterization of IL/MOF composites that were prepared by combining imidazolium-based ILs with MIL-53(Al) and compared the results with analogous composites of CuBTC and ZIF-8. These three different MOFs, MIL-53(Al), CuBTC, and ZIF-8, exhibit different physical, chemical, and textural properties: MIL-53(Al) is comprised of dicarboxylate groups and corner-sharing $AlO_4(OH)_2$ (μ_2-OH) chains, which result in a diamond-shaped network with 1D channels.[37] The narrow-pore form of MIL-53(Al) has channels with dimensions of 2.6×13.6 Å^2, while the large-pore form has channels with dimensions of 8.5×8.5 Å^2.[38] CuBTC is composed of dimeric copper tetracarboxylate units,[39] which form a cubic network with main pores (diameter: 9 Å), tetrahedral side pockets (5 Å), and windows in the pockets (3.5 Å).[40,41] On the other hand, ZIF-8 is composed of zinc ions with imidazole rings. It has narrow apertures (diameter: 3.4 Å), which are connected through large pores (11.6 Å).[42] MIL-53(Al) and CuBTC are hydrophilic, whereas ZIF-8 is hydrophobic. MIL-53(Al) exhibits exposed hydroxyl bridges, μ_2(O-H), and CuBTC has unsaturated metal sites, but ZIF-8 has neither open metal sites nor other exposed adsorption sites. For a comparison of the physical and chemical properties of these MOFs (and ILs), see the Supporting Information, Table S1 (and S2).

2.1. Characterization of the IL/MIL-53(Al) Composites

We have previously reported that the gas selectivity of an IL/MOF composite increases as the IL loading increases.[26,28] Thus, herein, we planned to use the highest-possible IL loading to generate the largest-possible improvement in CO_2 selectivity. At IL loadings above 30 wt%, the IL/MIL-53(Al) composites were formed as "muddy" products; thus, we inferred that 30 wt% IL loading was the incipient wetness limit of MIL-53(Al). Therefore, herein, the composites were prepared with a target IL loading of 30 wt%, and the actual IL loadings in the final products were determined by using XRF and ICP-MS analysis, as shown in Table 1 and Table 2, respectively. For the densities of the ILs, the IL loadings as vol.%, the percentage pore filling, and the number of IL molecules per unit cell of MIL-53(Al), see the Supporting Information, Table S3. Boron and fluorine elements in [BMIM][BF_4] were not detectable by using XRF; thus, we used ICP-MS analysis for the composite that included this IL, namely [BMIM][BF_4]/MIL-53(Al). Our results

Table 1. XRF results for MIL-53(Al) and the IL/MIL-53(Al) composites, and the IL loadings in the IL/MIL-53(Al) composites.

Sample	Formula	Conc. [wt%]	Calcd. IL loading [wt%]
pristine MIL-53(Al)	CHO	86.4	--
	Al	13.1	
	S	0.3	
[BMIM][PF_6]/MIL-53(Al)	CHO	87.9	25.4
	Al	9.1	
	P	2.6	
	S	0.3	
[BMIM][CF_3SO_3]/MIL-53(Al)	CHO	88.5	25.8
	Al	8.7	
	S	2.6	
[BMIM][SbF_6]/MIL-53(Al)	CHO	81.9	26
	Al	9.3	
	Sb	8.2	
	S	0.2	
	impurities	0.2	
[BMIM][NTf_2]/MIL-53(Al)	CHO	87.7	24.1
	Al	8.8	
	S	3.3	

Table 2. ICP-MS results of pristine MIL-53(Al) and [BMIM][BF_4]/MIL-53(Al).

Sample	Aluminum [ppm]	Boron [ppm]	IL loading [wt%]
pristine MIL-53(Al)	8.582	0.1823	--
[BMIM][BF_4]/MIL-53(Al)	9.4	1.388	25.8

showed that [BMIM][BF_4], [BMIM][PF_6], [BMIM][CF_3SO_3], [BMIM][SbF_6], and [BMIM][NTf_2] were loaded into MIL-53(Al) with compositions of 25.8, 25.4, 25.8, 26, and 24.1 wt%, respectively. The reasons for the lower IL loadings than the target amount (30 wt%) were nonhomogeneous mixing and the loss of the ILs on the walls of beaker whilst stirring with the magnetic stirrer.

The BET surface areas and pore volumes of pristine MIL-53(Al) and the IL/MIL-53(Al) composites are listed in Table 3. In general, the IL-incorporated MOFs exhibited a lower degree of N_2 adsorption than pristine MIL-53(Al), as shown in the Supporting Information, Figure S1. The decreases in the surface areas and pore volumes of all of the IL/MIL-53(Al) composites compared to those of pristine MIL-53(Al) confirmed that the pores in the MOFs had been partially occupied by the ILs upon loading. Pore-size-distribution analysis of pristine MIL-53(Al) and the IL/MIL-53(Al) composites confirmed that the composites had lower pore volumes than the pristine MOF (see the Supporting Information, Figure S2).

Table 3. BET surface areas and BJH cumulative adsorption pore volumes of the composites and pristine MIL-53(Al).

Sample	S_{BET} [$m^2 g^{-1}$]	V_{pore} [$cm^3 g^{-1}$]
MIL-53(Al)	472.70	0.189
[BMIM][BF_4]/MIL-53(Al)	28.26	0.043
[BMIM][PF_6]/MIL-53(Al)	39.59	0.059
[BMIM][CF_3SO_3]/MIL-53(Al)	44.64	0.070
[BMIM][SbF_6]/MIL-53(Al)	43.42	0.067
[BMIM][NTf_2]/MIL-53(Al)	51.45	0.078

SEM analysis of MIL-53(Al) and the IL/MIL-53(Al) composites showed that all of the samples were composed of needle-like agglomerates that were formed from cylindrical crystals (Figure 1 and the Supporting Information, Figure S3). The morphologies of the IL/MIL-53(Al) composites were similar to that of pristine MIL-53(Al) at all magnifications, thus indicating that the ILs did not alter the shape and size of the MOF crystals.

XRD analysis of pristine MIL-53(Al) and the IL/MIL-53(Al) composites, as well as their corresponding peak positions, are shown in Figure 2 and the Supporting Information, Table S4, respectively. Pristine MIL-53(Al) showed specific peaks at $2\theta =$ 8.8, 9.4, 12.3, 15.2, 17.7, and 26.6°, which indicated the coexistence of both narrow-pore (np) and large-pore (lp) structures.[43] [BMIM][BF_4]/MIL-53(Al) showed peaks at $2\theta = 8$, 8.5, 11.4, 14.9, 17.0, and 26.7°, which indicated that the MOF in this composite was in its lp form, with slightly shifted peaks. Although there were some minor shifts in the peaks, the other IL/MIL-53(Al) composites all demonstrated similar behavior to pristine MIL-53(Al). Apparently, all of the composites showed the coexistence of np and lp frameworks. We also observed that the intensities of the 2θ peaks of the IL/MIL-53(Al) composites were different than those of pristine MIL-53(Al). These differences could be the result of changes in the electronic environment in the MOF structure in the presence of an IL. The coexistence of np and lp frameworks, or the transformation into only np or lp structures, together with the changes in the intensities of the 2θ peaks, could be explained by the interactions between the ILs and the flexible nature of MIL-53(Al).

TGA results for the percentage weight changes and the derivative weights of pristine MIL-53(Al), the bulk ILs, and the IL/MIL-53(Al) composites are shown in Figure 3 and the Supporting Information, Figure S4. The corresponding T'_{onset} values are listed in the Supporting Information, Table S5. Although the samples were stored in a desiccator, almost all of them showed a weight loss owing to water content at about 100 °C, because of the hydrophilic nature of MIL-53(Al). Consistent with previous characterizations, the TGA results presented the following evidence of IL–MOF interactions: 1) all of the IL/MIL-53(Al) composites had lower T'_{onset} values than pristine MIL-53(Al) and the corresponding bulk ILs. The IL/MIL-53(Al) composites showed two steps, indicative of decomposition at different temperatures, whereas pristine MIL-53(Al) and the ILs each only showed one step. 2) All of the IL/MIL-53(Al) composites showed a greater weight loss than pristine MIL-53(Al) after heating to 700 °C under a N_2 atmosphere. 3) The exact IL loadings in the IL/MIL-53(Al) composites as obtained from the XRF results were higher or lower than the weight loss as calculated from their TGA results. For example, [BMIM][PF_6]/MIL-53(Al) was calculated to have an IL loading of 25.4 wt% from the XRF measurements. Pristine MIL-53(Al) lost 61.8 wt% of its initial weight, whilst the bulk [BMIM][PF_6] lost 99.7 wt% of its initial weight after heating to 700 °C (see the Supporting Information, Table S5). From the XRF results, we expected that the composite should lose 71.4 wt% of its weight, but instead we

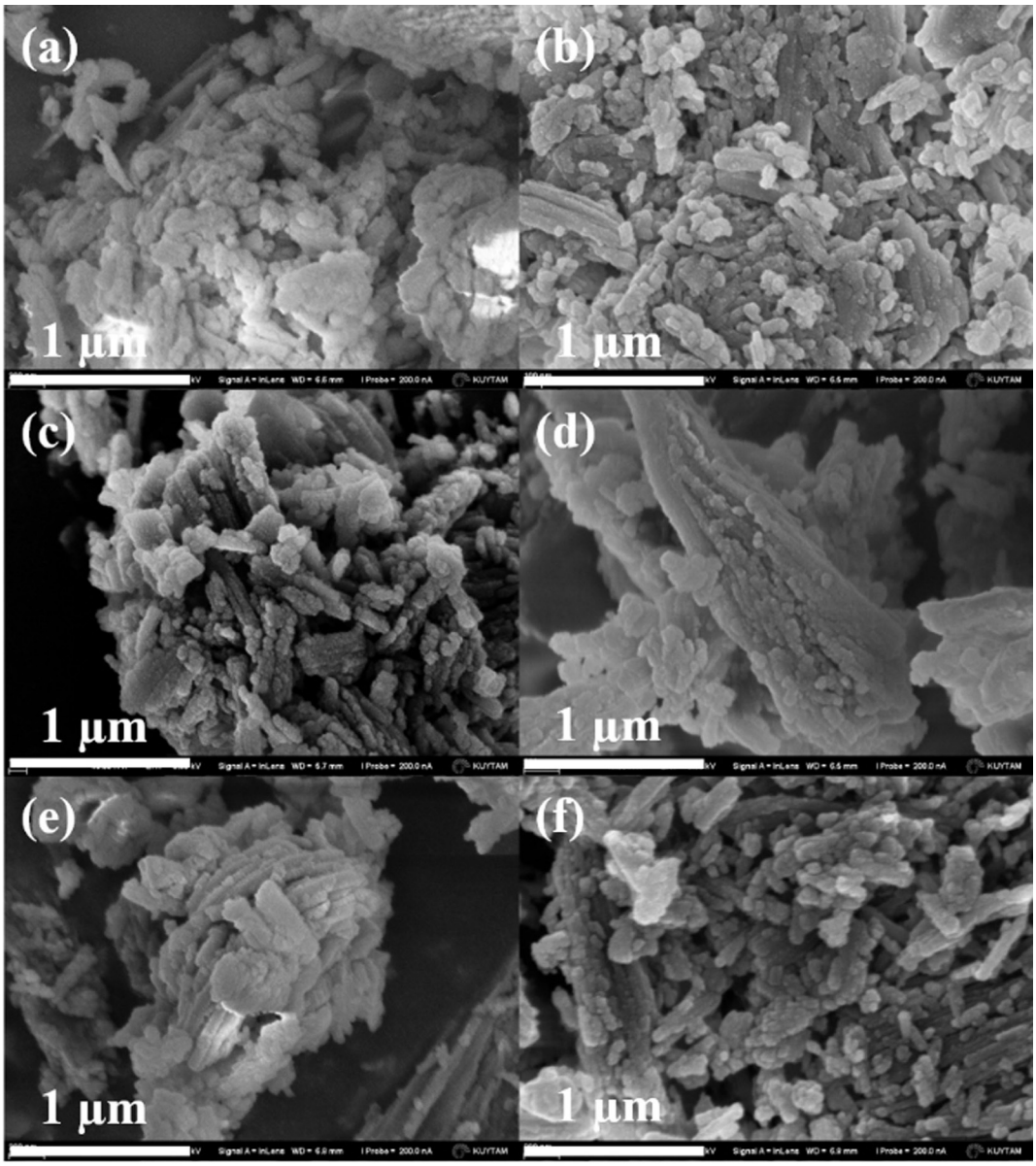

Figure 1. SEM images of a) pristine MIL-53(Al); b) [BMIM][BF_4]/MIL-53(Al); c) [BMIM][PF_6]/MIL-53(Al); d) [BMIM][CF_3SO_3]/MIL-53(Al); e) [BMIM][SbF_6]/MIL-53(Al); and f) [BMIM][NTf_2]/MIL-53(Al) (magnification: 100 k×).

only observed a loss as 64.6 wt% from the TGA results. This difference in weight loss between the XRF and TGA data could be attributed to a change in the individual decomposition mechanisms of the IL and the MOF in the IL/MOF composite. Thus, this change in the decomposition mechanisms indicated the presence of some strong molecular-level interactions between the IL and the MOF.

To clarify these interactions, we identified the major features in the IR spectra of all of the samples. The peak assignments were performed according to literature reports.[43–55] Figure 4 and the Supporting Information, Figures S5 and S6 show the IR spectra of pristine MIL-53(Al), the bulk ILs, and the IL/MIL-53(Al) composites. The Supporting Information, Tables S6 and S7 include the assignments of the vibrational IR bands of MIL-53(Al) and the bulk ILs, respectively. Changes in the MOF- and IL-originated peaks in the IL/MIL-53(Al) composites are listed in the Supporting Information, Tables S8 and S9, respectively, in which the colors denote the magnitude of the red or blue shifts. Both pristine MIL-53(Al) and the bulk ILs exhibited characteristic peaks in the 2000–400 cm^{-1} region; thus, it was challenging to determine whether the peaks belonged to the MOF or the IL. However, all of the ILs had characteristic peaks in the 3200–3000 cm^{-1} region (Figure 4a); thus this region was very useful for determining the IL-related peaks in the IL/MIL-53(Al) composites. Moreover, the Supporting Information, Figure S7 shows the μ_2(O–H) vibrations, which are characteristic of MIL-53(Al).

A detailed discussion on the IR spectra of the samples is provided in the Supporting Information. Briefly, the interactions between the IL molecules and the MIL-53(Al) framework could

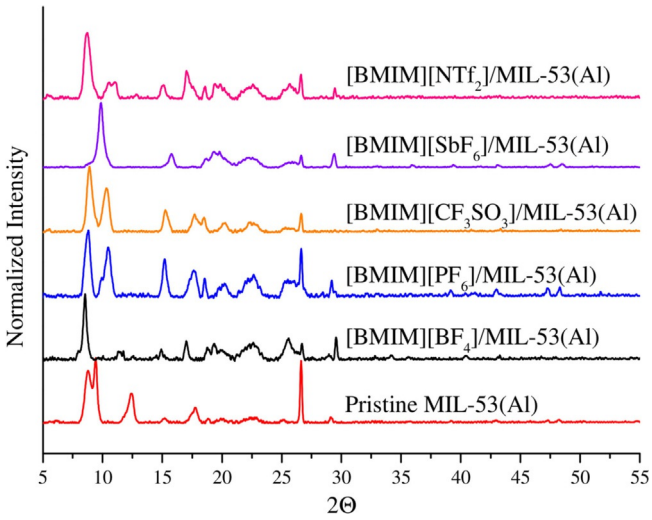

Figure 2. XRD patterns of (bottom to top) pristine MIL-53(Al), [BMIM][BF_4]/MIL-53(Al), [BMIM][PF_6]/MIL-53(Al), [BMIM][CF_3SO_3]/MIL-53(Al), [BMIM][SbF_6]/MIL-53(Al), and [BMIM][NTf_2]/MIL-53(Al).

be interpreted as follows: 1) based on the red shifts for the ν(C2–H), ν_{ss}(C4(H)–C5(H)), ν_{ss}(Al–O–Al), ν_{as}(Al–O–Al), δ(O–H), μ_2(O–H), ν_{as}(BF_4), and ν_{as}(PF_6) peaks, together with the unchanged ν(C–C) peaks of the organic linker, we inferred that [BMIM][BF_4] and [BMIM][PF_6] might be interacting with the aluminum backbone and with the bridging (O–H) group of MIL-53(Al), but not with the organic linker. 2) For [BMIM][CF_3SO_3], the ν_{ss}(SO_3) and ν_{as}(SO_3) peaks were both red-shifted, whereas the ν(C4(H)–C5(H)) and ν(C2–H) peaks were blue-shifted, and the ν(Al–O–Al), ν(C–C), and δ(C–C–C) peaks were unchanged. Therefore, [BMIM][CF_3SO_3] and MIL-53(Al) might have interacted through the SO_3 side of the anion, thereby causing the CF_3 side of the anion to become stronger, as evidenced by a blue shift of the ν_{as}(CF_3) peak. 3) The shifts for the ν(C4(H)–C5(H)), μ_2(O–H), ν(C–C), δ(C–C–C), and ν_{ss}(Al–O–Al) peaks in the spectra of [BMIM][SbF_6]/MIL-53(Al) and [BMIM][NTf_2]/MIL-53(Al) were smaller than the spectroscopic resolution, whilst ν(C2–H) was red-shifted in both cases. Moreover, the ν(SbF_6) peak in [BMIM][SbF_6] and the ν(C–S) peak in [BMIM][NTf_2] were slightly blue-shifted. These results might indicate that the anions in [BMIM][SbF_6] and [BMIM][NTf_2] interacted with MIL-53(Al), thereby strengthening the Sb–F and C–S bonds, as indicated by the blue shifts of the ν(SbF_6) and ν(C–S) peaks. Taken together, these results showed that all of the ILs and MIL-53(Al) strongly interacted with each other in the corresponding composite samples. Based on these data, we inferred that the ILs with small anions, [BMIM][BF_4] and [BMIM][PF_6], preferred to be located near the aluminum backbone of MIL-53(Al) and the μ_2(O–H) moiety of MIL-53(Al), similar to FTIR results for the [BMIM][$MeSO_4$]/MIL-53(Al) composite.[33] However, the bulky ILs, [BMIM][CF_3SO_3], [BMIM][SbF_6], and [BMIM][NTf_2], preferred to be located near to the organic linker. Our findings are consistent with previous reports.[56–58]

2.2. Gas Adsorption and Gas-Separation Performance of the IL/MIL-53(Al) Composites

The CO_2, CH_4, and N_2 adsorption isotherms of pristine MIL-53(Al) and the IL/MIL-53(Al) composites were measured at 25 °C and 0.1–5 bar (Figure 5). The dual-site Langmuir model was used to fit the adsorption isotherms, and the fit parameters are given in the Supporting Information, Table S10. All of the IL/MIL-53(Al) composites showed a lower CO_2, CH_4, and N_2 uptake than pristine MIL-53(Al) over the entire pressure range. This decrease was expected, because the pore volumes of the IL/MIL-53(Al) composites were lower than that of pristine MIL-53(Al) (Table 3). The CO_2, CH_4, and N_2 solubilities of the bulk ILs were estimated by using COSMO-RS calculations, which are widely used to predict and screen the solubility of gases in ILs.[59–63] According to these results (see the Supporting Information, Figure S8), the order of the gas solubilities in the bulk ILs was quite different to that of the gas uptakes by the corresponding IL/MOF composites. This dissimilarity was attributed to interactions between the IL and MIL-53(Al), which resulted in a change in the affinity of the corresponding IL towards the gas molecules. Moreover, to show the reversibility of the adsorption, we measured the adsorption/desorption isotherms of pristine MIL-53(Al) and the IL/MIL-53(Al) composites for CO_2, CH_4, and N_2 (see the Supporting Information, Figure S9). These results did not show any hysteresis upon desorption of the gases, thus indicating that our composites offer a high potential for applications in separation processes.

The ideal selectivities of the composites were calculated by dividing the adsorption amount of the more adsorbed gas by that of the less adsorbed gas. To better evaluate the impact of IL incorporation on the CO_2 selectivity of MIL-53(Al), we calculated the normalized selectivities of the IL/MIL-53(Al) composites by dividing the selectivity of the composite by the selectivity of pristine MIL-53(Al) at the same pressure. The normalized CO_2/CH_4 and CO_2/N_2 selectivities of the IL/MIL-53(Al) composites are shown in Figure 6. [BMIM][BF_4]/MIL-53(Al), [BMIM][PF_6]/MIL-53(Al), and [BMIM][$MeSO_4$]/MIL-53(Al) all contained ILs with small anions, as shown in the Supporting Information, Table S2, and they afforded higher CO_2/CH_4 selectivities at all pressures compared to the composites that contained bulky ILs (Figure 6a). These composites also afforded higher CO_2/CH_4 selectivities than that of MIL-53(Al) over the entire pressure range. The IR spectra of the IL/MIL-53(Al) composites showed that the smaller anions, $[BF_4]^-$, $[PF_6]^-$, and $[MeSO_4]^-$, were located near the aluminum backbone and the bridging O–H group of MIL-53(Al), instead of the organic linkers.[33] This preference might be the reason for the higher CO_2 selectivity. Gupta et al. reported molecular simulations which showed that smaller anions $[BF_4]^-$, $[PF_6]^-$, and $[SCN]^-$ preferred locations near the metal cluster of IRMOF-1 (also known as MOF-5), and that these anions increased the selectivity of IRMOF-1 for CO_2 more than the $[Tf_2N]^-$ anion, which was located proximal to the phenyl rings of IRMOF-1.[56] Herein, [BMIM][BF_4]/MIL-53(Al), [BMIM][PF_6]/MIL-53(Al), and [BMIM][$MeSO_4$]/MIL-53(Al)[33] showed similar behavior: their normalized selectivities increased up to 0.2–0.4 bar and then decreased on further in-

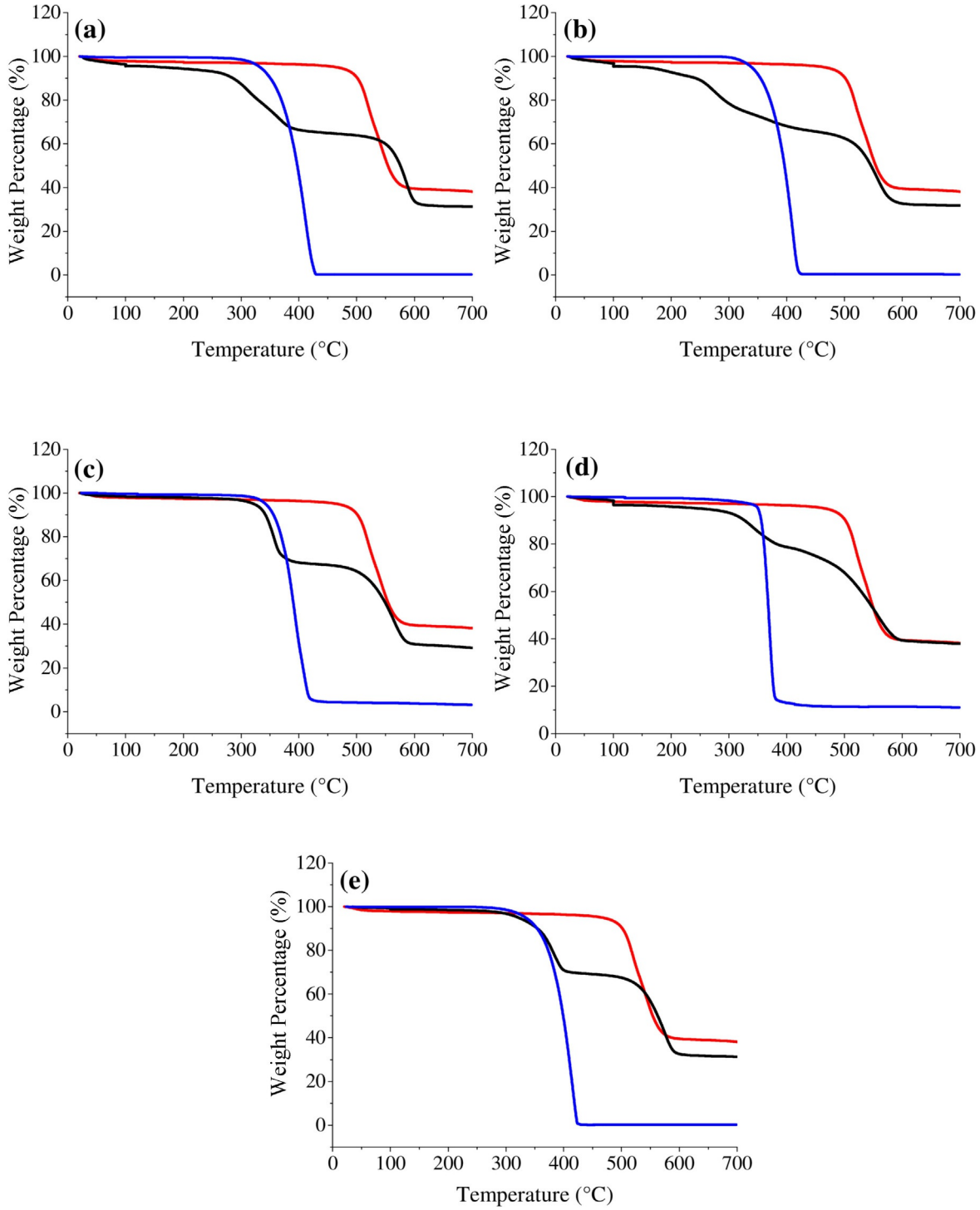

Figure 3. TGA curves of MIL-53(Al) (red lines), the bulk ILs (blue lines), and the IL/MIL-53(Al) composites (black lines)where the IL is: a) [BMIM][BF_4]; b) [BMIM][PF_6]; c) [BMIM][CF_3SO_3]; d) [BMIM][SbF_6]; and e) [BMIM][NTf_2].

creasing the pressure. [BMIM][PF_6]/MIL-53(Al) showed the highest normalized CO_2/CH_4 selectivity among the IL/MIL-53(Al) composites that were tested: 2.8-times that of pristine MIL-53(Al) at 0.3 bar. [BMIM][BF_4]/MIL-53(Al), [BMIM][PF_6]/MIL-53(Al), and [BMIM][$MeSO_4$]/MIL-53(Al) also exhibited higher CO_2/N_2 selectivities than the other composites and pristine MOF (Figure 6b). Furthermore, among the composites that were considered, [BMIM][$MeSO_4$]/MIL-53(Al) showed the highest normalized CO_2/N_2 selectivity: 3.3- and 2.4-times higher than that of pristine MIL-53(Al) at 0.01 and 1 bar, respectively.

For a representative comparison, we measured the isosteric heats of adsorption (Q_{st}) for CO_2, CH_4, and N_2 as a function of gas uptake in MIL-53(Al) and [BMIM][PF_6]/MIL-53(Al). The fitting parameters to the virial-type thermal adsorption equation for

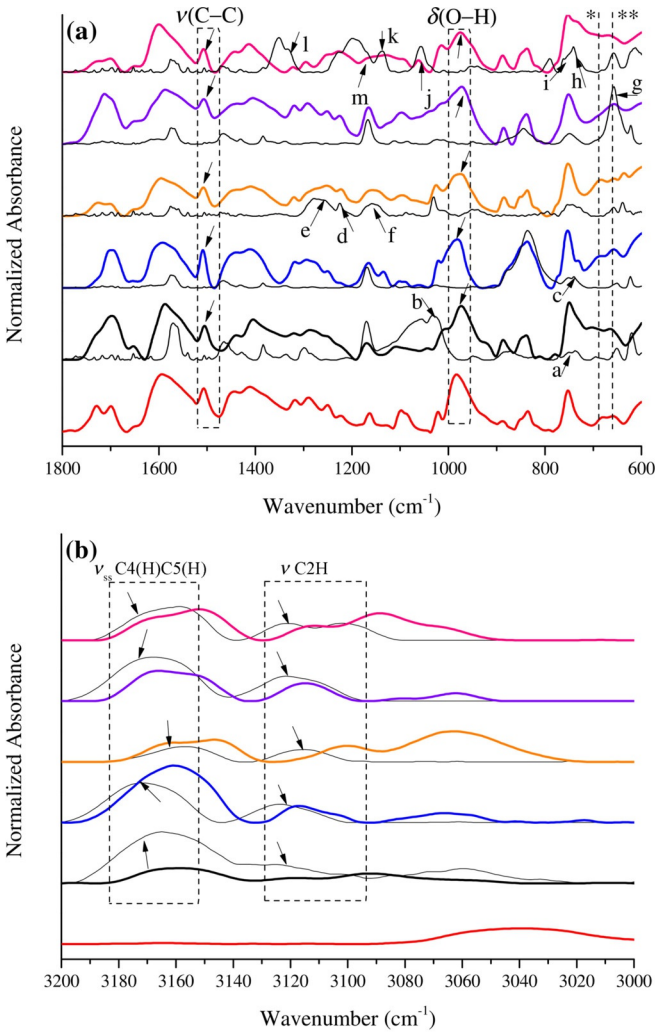

Figure 4. IR spectra of pristine MIL-53(Al), the bulk ILs, and the IL/MIL-53(Al) composites within the regions a) 1800–600 cm^{-1} and b) 3200–3000 cm^{-1}. Red: pristine MIL-53(Al); black: [BMIM][BF_4]/MIL-53(Al); blue: [BMIM][PF_6]/MIL-53(Al); orange: [BMIM][CF_3SO_3]/MIL-53(Al); violet: [BMIM][SbF_6]/MIL-53(Al); pink: [BMIM][NTf_2]/MIL-53(Al). The overlapping thin black lines denote the IR spectra of the corresponding bulk ILs: $\nu_{ss}(BF_4)$ (a), $\nu_{as}(BF_4)$ (b), $\nu_{as}(PF_6)$ (c), $\nu_{ss}(SO_3)$ (d), $\nu_{as}(SO_3)$ (e), $\nu_{as}(CF_3)$ (f), $\nu(SbF_6)$ (g), ν(C–S) (h), ν_{ss}(S–N) (i), ν_{as}(S–N) (j), $\nu_{ss}(SO_2)$ (k), $\nu_{as}(SO_2)$ (l), $\nu_{as}(CF_3)$ (m), ν_{as}(Al–O–Al) (*), and ν_{ss}(Al–O–Al) (**). as = asymmetrical stretch, ss = symmetrical stretch.

the CO_2, CH_4, and N_2 isotherms at 10 and 20 °C are shown in the Supporting Information, Table S11. Accordingly, MIL-53(Al) and [BMIM][PF_6]/MIL-53(Al) had Q_{st} values within the range 21–33 kJ mol^{-1} and 28–35 kJ mol^{-1} for CO_2, 16–17 kJ mol^{-1} and 11–14 kJ mol^{-1} for CH_4, and 12–13 kJ mol^{-1} and 10–11 kJ mol^{-1} for N_2, respectively. These ranges were consistent with the previously reported Q_{st} values for [BMIM][$MeSO_4$]/MIL-53(Al).[33] The higher Q_{st} value of the composite for CO_2 compared to the pristine MOF indicated that its affinity for CO_2 molecules was enhanced, with a corresponding decrease in the Q_{st} values for CH_4 and N_2. This result further clarified the improvement in the CO_2/CH_4 and CO_2/N_2 selectivities upon the incorporation of [BMIM][PF_6] into MIL-53(Al).

2.3. Effect of the IL and MOF on the CO_2 Selectivity of the IL/MOF Composites

To elucidate the effect of IL incorporation on MOFs with different properties, we compared the gas-separation performances of the [BMIM][BF_4]/MIL-53(Al) and [BMIM][PF_6]/MIL-53(Al) composites with those of previously reported composites [BMIM][BF_4]/CuBTC,[26] [BMIM][PF_6]/CuBTC,[27] [BMIM][BF_4]/ZIF-8,[28] and [BMIM][PF_6]/ZIF-8 (all of these composites had comparable near-saturation IL loadings).[29] The ideal CO_2/CH_4 and CO_2/N_2 selectivities of [BMIM][BF_4]- and [BMIM][PF_6]-incorporated CuBTC,[26,27] ZIF-8,[28,29] and MIL-53(Al) are shown as a function of pressure in the Supporting Information, Figure S10. As shown in Figure 7 a, b, the incorporation of [BMIM][BF_4] and [BMIM][PF_6] into CuBTC decreased the CO_2/CH_4 selectivity of the MOF, which was attributed to the open metal sites in CuBTC.[64,65] Accordingly, the interaction of the open metal sites of the MOF with the IL molecules prevented the subsequent interaction of CO_2 molecules with the open metal sites, and so the composite material did not exhibit any enhancement in CO_2 selectivity. On the other hand, the incorporation of [BMIM][BF_4] and [BMIM][PF_6] into ZIF-8 enhanced its CO_2/CH_4 selectivity at low pressures (2.5- and 4-times higher than that of pristine ZIF-8, respectively), but, at high pressures, the presence of an IL did not cause a significant change in the CO_2/CH_4 selectivity of ZIF-8. The incorporation of [BMIM][BF_4] and [BMIM][PF_6] into MIL-53(Al) improved the CO_2/CH_4 selectivity of the MOF over the entire pressure range. The normalized CO_2/CH_4 selectivities of the MIL-53(Al) composites were 1.6–2.6 and 1.6–2.8 with [BMIM][BF_4] and [BMIM][PF_6], respectively. Taken together, these results suggested that the incorporation of [BMIM][BF_4] and [BMIM][PF_6] improved the CO_2/CH_4 selectivity of MIL-53(Al), whilst only enhancing the selectivity of ZIF-8 at low pressures, and not causing any remarkable change in the selectivity of CuBTC.

Similarly, we also compared the CO_2/N_2 selectivities of these composites. Thus, the incorporation of [BMIM][BF_4] into CuBTC decreased its CO_2/N_2 selectivity, as was the case for CO_2/CH_4 selectivity. However, the incorporation of [BMIM][PF_6] into CuBTC slightly increased its CO_2/N_2 selectivity at low pressures ($<$ 0.3 bar). The incorporation of [BMIM][BF_4] and [BMIM][PF_6] into ZIF-8 enhanced its CO_2/N_2 selectivity at low pressures (2.7- and 3.6-times that of ZIF-8, respectively). However, at high pressures, the incorporation of both ILs into ZIF-8 did not cause any notable improvement in CO_2/N_2 selectivity. [BMIM][PF_6]/ZIF-8 showed higher CO_2/N_2 selectivity than [BMIM][BF_4]/ZIF-8, which may attributed to the relative polarities of the anions: CO_2 molecules are nonpolar and, thus, $[PF_6]^-$, which is less polar than $[BF_4]^-$, is more favorable for CO_2.[66] The incorporation of [BMIM][BF_4] and [BMIM][PF_6] into MIL-53(Al) enhanced its CO_2/N_2 selectivity by 3.2- and 2.1-times compared to that of MIL-53(Al), respectively. At high pressures, the incorporation of these ILs into MIL-53(Al) resulted in a greater degree of improvement in CO_2/N_2 selectivity compared to the corresponding composites with ZIF-8 and CuBTC MOFs. Of these two ILs, the incorporation of [BMIM][BF_4] into MIL-53(Al) resulted in a larger increase in CO_2/N_2 selectivity compared to the incorpora-

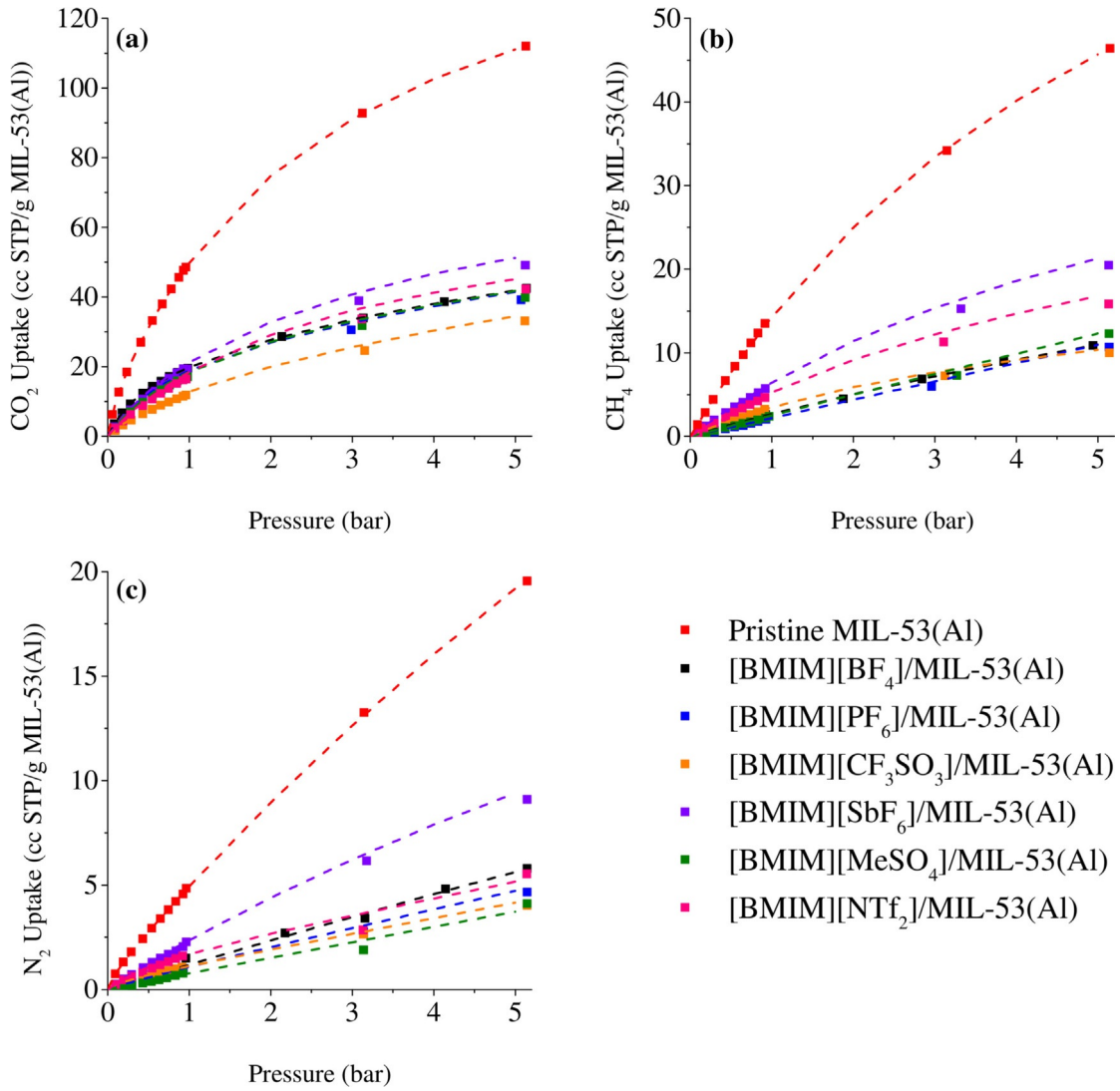

Figure 5. CO_2 (a), CH_4 (b), and N_2 (c) uptakes of pristine MIL-53(Al) and the IL/MIL-53(Al) composites. Dashed lines represent the fitted isotherms. The data for [BMIM][$MeSO_4$]/MIL-53(Al) are reprinted with permission from Ref. [33].

tion of [BMIM][PF_6], which may be attributed to the relative hydrophilicities of the ILs and MOFs: ZIF-8 and [BMIM][PF_6] are both hydrophobic, whereas MIL-53(Al) and [BMIM][BF_4] are both hydrophilic. The lower polarity of the $[PF_6]^-$ anion could be favorable for CO_2 adsorption onto hydrophobic ZIF-8, but unfavorable for adsorption onto hydrophilic MIL-53(Al), which could affect the CO_2 selectivity of the IL/MIL-53(Al) composite. Overall, these results indicated that the incorporation of [BMIM][BF_4] and [BMIM][PF_6] enhanced the CO_2/N_2 selectivities of MIL-53(Al) and ZIF-8, and that MIL-53(Al) offers a more versatile platform than its counterparts.

Next, we performed a comprehensive comparison of the CO_2/CH_4 and CO_2/N_2 selectivities of the IL/MIL-53(Al) composites with those of selected pristine MOFs to assess the potential of IL-incorporated MIL-53(Al) composites for CO_2 separation applications, such as natural gas and flue gas purification. Thus, we calculated the ideal selectivities of our IL/MIL-53(Al) composites as the ratio of their gas uptake. To be able to use the gas uptakes at the same pressure, we first fitted the gas adsorption data to the dual-site Langmuir model and used these fits to determine the corresponding uptake value for each gas at any given pressure. Furthermore, we also used ideal adsorption solution theory (IAST) to calculate the mixture selectivities for different gas compositions, such as $CO_2/CH_4 = 10:90$, $CO_2/N_2 = 15:85$, $CO_2/CH_4 = 50:50$, and $CO_2/N_2 = 50:50$, to allow for comparison with the data shown in Table 4. Our results showed that the loading of ILs that contained small anions, $[BF_4]^-$, $[PF_6]^-$, and $[MeSO_4]^-$, into MIL-53(Al) improved its CO_2 selectivity over CH_4 and N_2. For example, pristine MIL-53(Al) had a lower ideal CO_2/N_2 selectivity than Cd–L, Cu–BTTri, Fe–BTT, [Fe_2(BPEB)$_3$], [Ni(BPEB)], rho-ZMOF, sod-ZMOF, and ZIF-81, as shown in Table 4. On the other hand, the [BMIM][$MeSO_4$]/MIL-53(Al)[33] composite exhibited the highest CO_2/N_2 selectivity among all of the IL/MIL-53(Al) composites that we considered (24.2), and this value is higher than those for all of the MOFs reported in Table 4. This comparison indi-

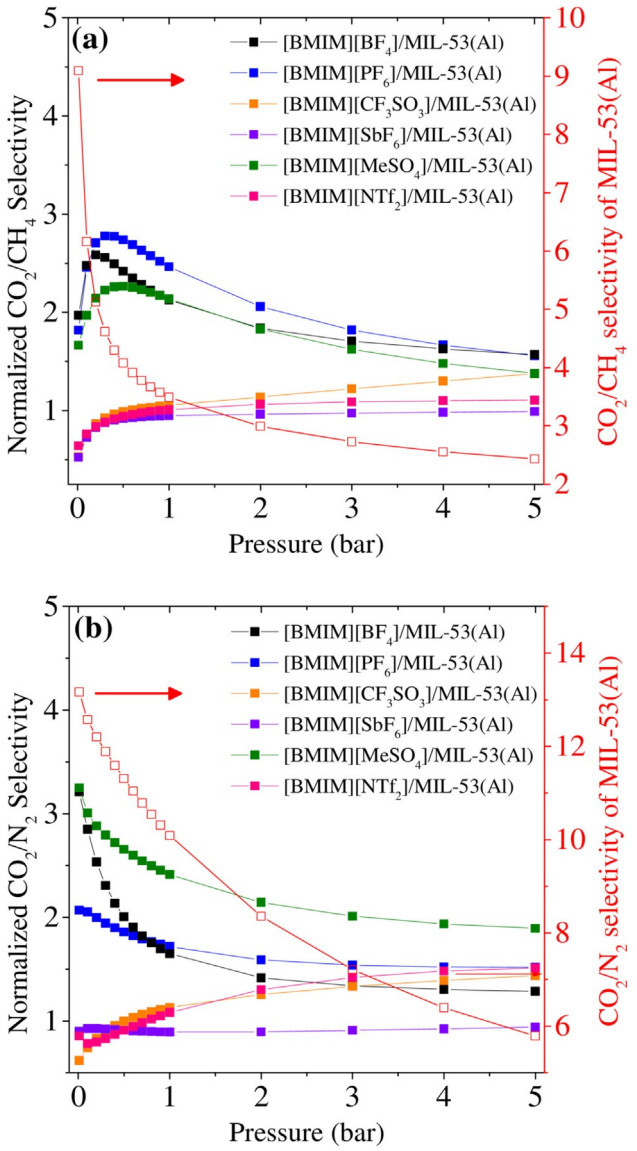

Figure 6. Plots of the normalized selectivities of the IL/MIL-53(Al) composites for CO_2/CH_4 (a) and CO_2/N_2 (b) as a function of pressure. The left-hand *y* axis represents the normalized selectivities of the IL/MIL-53(Al) composites, which were calculated by dividing the selectivities of the composites by the selectivity of MIL-53(Al) at the same pressure. The right-hand *y* axis shows the ideal selectivity of pristine MIL-53(Al). The data for [BMIM][$MeSO_4$]/MIL-53(Al) are reprinted with permission from Ref. [33].

cated that MIL-53(Al) represents an excellent platform for IL incorporation to develop new IL/MOF composites with exceptionally high CO_2 selectivity.

Finally, we compared the CO_2/N_2 selectivities for the IL/MIL-53(Al) composites with those of previously reported IL/MOF composites: [BMIM][OAc]/ZIF-8 and [EMIM][OAc]/ZIF-8.[31] The [BMIM][OAc]/ZIF-8 composites with IL loadings of 10, 20, and 30 wt% were reported to have CO_2/N_2 selectivities of less than 15 at 1 bar and 30 °C. However, at 0.1 bar and 30 °C, [BMIM][OAc]/ZIF-8 (20 wt%) had an ideal CO_2/N_2 selectivity of 54. Although their working temperature (30 °C) was slightly higher than ours (25 °C), these data might offer a beneficial benchmark for IL/MOF composites in the literature. [BMIM][BF_4]/MIL-53(Al), [BMIM][PF_6]/MIL-53(Al), and [BMIM][$MeSO_4$]/MIL-53(Al) had ideal CO_2/N_2 selectivities of 42.3, 27.3, and 42.2 at 0.1 bar and 25 °C, and 16.8, 17.3, and 24 at 1 bar and 25 °C, respectively.[33] Thus, these IL/MIL-53(Al) composites had higher ideal CO_2/N_2 selectivities than those of [BMIM][OAc]/ZIF-8 (10, 20, and 30 wt%) at 1 bar and [BMIM][OAc]/ZIF-8 (10 and 30 wt%) at 0.1 bar, but lower than that of [BMIM][OAc]/ZIF-8 (20 wt%) at 0.1 bar. A loading of 10 wt% in the [EMIM][OAc]/ZIF-8 composite gave the highest ideal CO_2/N_2 selectivity at 0.1 bar, compared to other wt% loadings in the same composite. At 1 bar, the ideal CO_2/N_2 selectivities of all of the IL loadings of this sample were lower than 7.5. According to these values, [BMIM][BF_4]/MIL-53(Al), [BMIM][PF_6]/MIL-53(Al), and [BMIM][$MeSO_4$]/MIL-53(Al) all had higher ideal CO_2/N_2 selectivities than those of [EMIM][OAc]/ZIF-8 (10, 20, and 30 wt%) at 0.1 and 1 bar. Overall, our IL/MIL-53(Al) composites with small anions offer greater ideal CO_2/N_2 selectivities under specific conditions, which further demonstrates the potential of MIL-53(Al) as a platform for the design of high-performance IL/MOF composites.

Table 4. Comparison of the CO_2 selectivities of a range of MOFs with the IL/MIL-53(Al) composites.

MOF	CO_2/CH_4 selectivity	CO_2/N_2 selectivity	*T* [°C]	*P* [bar]	Ref.
BUT-10	5.1[a]	22.9[c]	25	1	[67]
Cd-L	--	18.4	0	1	[68]
Cu–BTTri	--	21	25	1	[69]
Fe–BTT	--	10.8	25	1	[70]
[Fe_2(BPEB)$_3$]	--	20	25	1	[71]
LIFM-10	4.3[b]	14.5[c]	25	1	[72]
[Ni(BPEB)]	--	19	25	1	[71]
NPC-6	7.3[d]	26.4[d]	20	1	[73]
rho-ZMOF	--	22.6	25	1	[74]
SNU-151′	7.2[d]	--	25	1	[75]
sod-ZMOF	--	20.4	25	1	[74]
TMU-5	--	23.2[d]	25	1	[76]
ZIF-79	5.4[e]	23.2[e]	25	1	[77]
ZIF-81	5.7	23.8	25	1	[77]
ZIF-95	4.3[b]	18[b]	25	1	[78]
MIL-53(Al)	3.5 7[a] 6.3[d]	10.1 22.8[c] 21.1[d]	25	1	this work
IL/MIL-53(Al) composites	3.3–8.6 4.7–17.2[a] 4.7–15.5[d]	9–24.2 14–39.5[c] 14.5–36.1[d]	25	1	this work

[a] Calculated by using ideal adsorbed solution theory (IAST) for CO_2/CH_4 (10:90, v/v). [b] Calculated from the breakthrough experiments by using equimolar CO_2/CH_4 and CO_2/N_2 mixtures. [c] Calculated by using IAST for CO_2/N_2 (15:85, v/v). [d] Calculated by using IAST with 50:50 (v/v) inlet gas compositions of CO_2/CH_4 and CO_2/N_2. [e] Calculated from the slope of the adsorption isotherm at low pressure; unless otherwise noted, ideal selectivities are reported. BUT = Beijing University of Technology, BTTri = 1,3,5-tris(1*H*-1,2,3-triazol-5-yl)benzene, BTT = benzene-1,3,5-tristetrazole, BPEB = 1,4-bis[(1H-pyrazol-4-ylethynyl) benzene, LIFM = Lehn Institute of Functional Materials, NPC = nanoporous cage, rho-ZMOF = rhodonite zeolite-like metal–organic framework, sod-ZMOF = sodalite zeolite-like metal–organic framework, SNU = Seoul National University, TMU = Tarbiat Modares University.

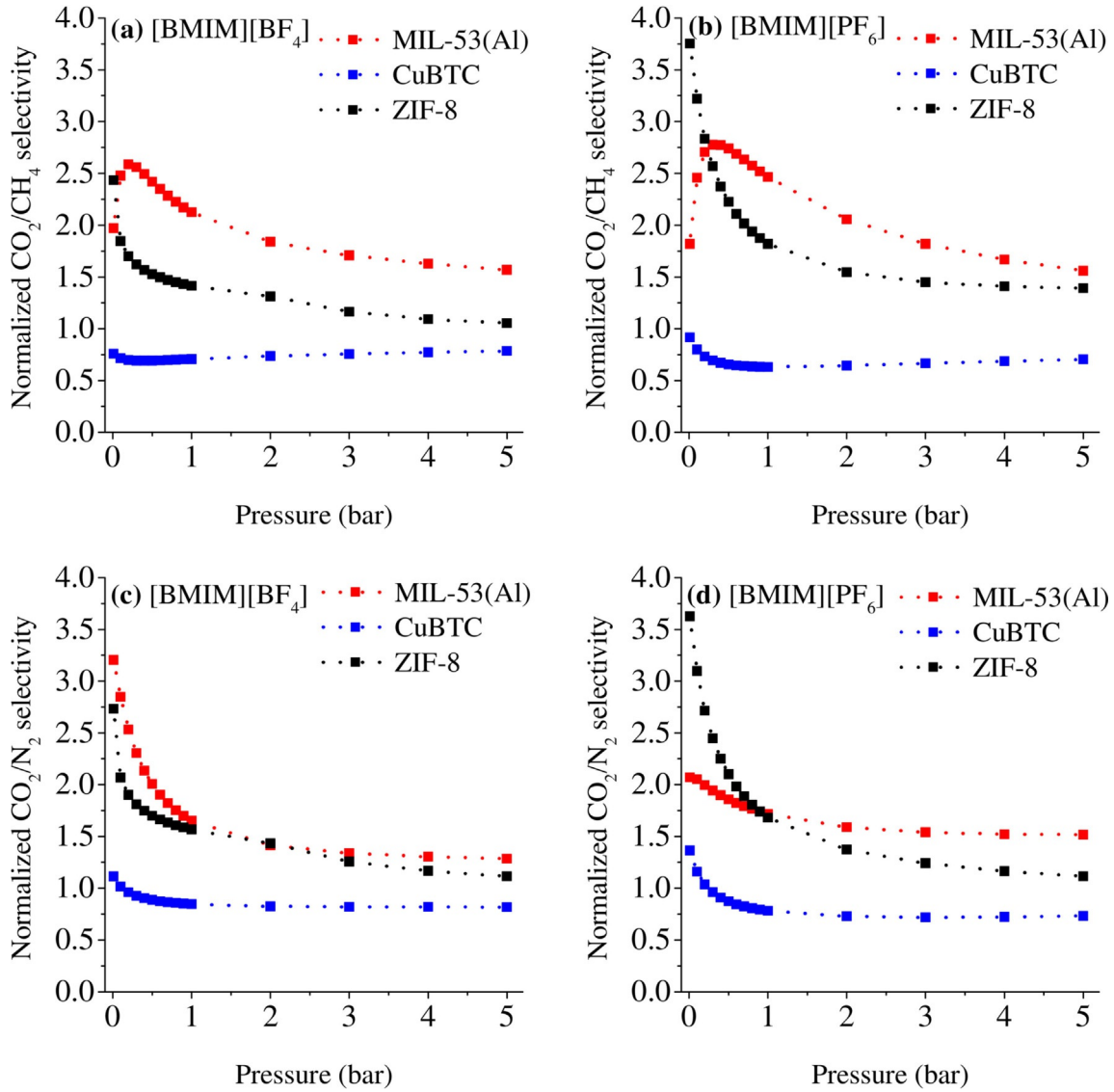

Figure 7. Plots of the normalized CO_2/CH_4 and CO_2/N_2 selectivities of the [BMIM][BF_4]- (a, c) and [BMIM][PF_6]-incorporated MIL-53(Al) composites (b, d), as well as CuBTC[26,27] and ZIF-8,[28,29] as a function of pressure.

3. Conclusions

We have studied five different IL-loaded MIL-53(Al) composite materials. The ILs consisted of $[BMIM]^+$ cations and anions with different chemical and physical properties, such as hydrophilicity/hydrophobicity and bulkiness. The newly synthesized IL/MIL-53(Al) composites were characterized in detail and we found that the ILs had been successfully incorporated into the MIL-53(Al) framework. By comparing the IR spectra of the composites with that of pristine MIL-53(Al), we concluded that ILs with small anions, [BMIM][BF_4] and [BMIM][PF_6], were preferably located near the aluminum backbone and the μ_2(O–H) moiety of the MIL-53(Al) framework, whereas ILs with bulky anions were preferably located near the organic linkers. CO_2, CH_4, and N_2 adsorption measurements were performed within the pressure range of 0.1–5 bar, and [BMIM][BF_4]/MIL-53(Al), [BMIM][PF_6]/MIL-53(Al), and [BMIM][$MeSO_4$]/MIL-53(Al) showed the highest CO_2/CH_4 and CO_2/N_2 selectivities among all of the samples that were tested. The highest level of improvement in terms of CO_2/CH_4 selectivity was observed for [BMIM][PF_6]/MIL-53(Al), which exhibited a selectivity that was 2.8-times higher that of pristine MIL-53(Al) at 0.3 bar. [BMIM][$MeSO_4$]/MIL-53(Al) exhibited the highest CO_2/N_2 selectivity, which varied between 1.9- and 3.3-times higher than that of MIL-53(Al) within the examined pressure range. The effects of using different ILs and MOFs were studied by comparing the incorporation of [BMIM][BF_4] and [BMIM][PF_6] into MIL-53(Al), CuBTC, and ZIF-8. Because CO_2 molecules typically prefer open metal sites, the incorporation of both ILs decreased the CO_2 separation performance of CuBTC. ZIF-8 showed a better performance with [BMIM][PF_6] than it does with [BMIM][BF_4] for both CO_2/CH_4 and CO_2/N_2 selectivities. This result was attributed to the weaker polarity of the $[PF_6]^-$ anion, which improved the CO_2 attraction because CO_2 molecules are nonpolar.

This study suggests that the chemical and physical properties of both ILs and MOFs and the interactions between them should be taken into consideration for the design of new IL/MOF composites with high CO_2 separation potentials. This study also presents MIL-53(Al) as a versatile platform for IL/MOF composites and will hopefully pave the way for further studies to determine the best IL and MOF couples for the development of new IL/MOF composites with high CO_2 separation performance.

Experimental Section

Materials

MIL-53(Al) (Basolite A100) and all of the ILs were purchased from Sigma–Aldrich and stored in an argon-filled glovebox prior to use (Labconco). Acetone (≥99.5 vol.%) was purchased from Sigma–Aldrich. CO_2 (99.9 vol. %), CH_4 (99.95 vol.%), and N_2 (99.998 vol.%) were purchased from Linde Gas Company; He (99.999 vol.%), which was used for the gas adsorption measurements, was purchased from the Messer Group.

Sample Preparation

Prior to the sample preparation, MIL-53(Al) was dehydrated overnight under vacuum at 200 °C. IL/MOF composites with 30 wt% IL loading were prepared open to air by using the wet-impregnation method, as reported previously.[26] First, the IL was dissolved in acetone (20 mL) by stirring under ambient conditions for 1 h. Then, dehydrated MIL-53(Al) powder was added to the solution and the mixture was stirred at 35 °C open to air until the acetone had completely evaporated. The resulting IL/MOF composites were dried at 105 °C overnight and stored in a desiccator to minimize the effect of humidity and the presence of impurities.

X-ray Fluorescence (XRF)

A Bruker S8 Tiger spectrometer was used for the elemental analysis of pristine MIL-53(Al) and the IL/MIL-53(Al) composites. An X-ray tube with a 4 kW rhodium anode was used for the analysis, which was performed under helium atmosphere. SpectraPlus Eval2 V2.2.454 software was used for the data interpretation.

Inductively Coupled Plasma Mass Spectrometry (ICP-MS)

The concentrations of boron and aluminum atoms in the samples were measured by using an Agilent 7700x ICP-MS (Agilent Technologies Inc., Tokyo, Japan). First, a small amount of pristine MIL-53(Al) or [BMIM][BF_4]/MIL-53(Al) (ca. 5 mg) was dissolved in a concentrated aqueous solution of HNO_3 (65%, 6 mL). Then, the solution was diluted with deionized water (50 mL). ICP-MS analysis was performed by using a MicroMist microuptake glass concentric nebulizer, an inert-sample-introduction kit with a sapphire injector (inner diameter: 2.5 mm; Agilent 7700 series, Agilent Technologies, Germany), and nickel sampler/skimmer cones. Instrument optimization was performed prior to use by using a tuning solution (1 $\mu g L^{-1}$) to ensure the short-term stability of the instrument. External calibration solutions were prepared by using Spex Certiprep multielement calibration standards (CLMS-2AN for Al, CLMS-4 for B). Calculations were performed by using the MassHunter software.

Brunauer–Emmett–Teller (BET) Surface Area and Barrett–Joyner–Halenda (BJH) Pore-Volume Analyses

A Micromeritics TriStar II 3020 analyzer was used for the N_2-physisorption analysis. First, pristine MIL-53(Al) and the IL/MIL-53(Al) composites were activated at 150 °C and 100 °C, respectively, for 10 h under vacuum prior to the measurements. Then, the samples were cooled to −196 °C by using liquid nitrogen and free-space measurements were performed by using helium gas. Next, N_2-adsorption isotherms were recorded between $\times 10^{-6}$ and 1 bar at −196 °C. The surface area of each sample was estimated by fitting the nitrogen-adsorption isotherms to the BET equation, by using the relative pressure (P/P_0) range 0.06–0.3. The pore-size distributions (PSDs) were calculated from the adsorption branch of the isotherm by using the Barrett–Joyner–Halenda (BJH) method.

Scanning Electron Microscopy

SEM images of pristine MIL-53(Al) and the IL/MIL-53(Al) composites were obtained by using a Zeiss Evo LS 15 scanning electron microscope. To mitigate the problem of charging the materials, the samples were first placed onto carbon tape and then their surfaces were coated with carbon. The analysis was performed under vacuum at an accelerating voltage of 3 kV, with working distances of 4.1–4.5 mm, and magnifications of 100, 50, and 12.5 k×.

X-Ray Diffraction Spectroscopy

XRD patterns were obtained by using a Bruker D8 Phaser instrument with a Lynxeye detector at a slit width of 1 mm. An X-ray generator with a Cu Kα1 radiation source (1.54060 Å) was operated at a voltage of 30 kV and a current of 10 mA. The analysis was performed within the range $2\theta = 5$–$90°$ with a resolution of 0.0204°.

Thermogravimetric Analysis (TGA)

A TA Instruments Q500 Thermogravimetric Analyzer with a platinum pan was used for the TGA experiments. First, approximately 15 mg of each sample, pristine MIL-53(Al), the bulk ILs, and the IL/MIL-53(Al) composites was placed onto the platinum pan, heated to 100 °C at a ramp rate of 5 °C min^{-1}, and held at this temperature for 8 h. Then, the temperature was further increased to 700 °C at a rate of 2 °C min^{-1}. All of the measurements were performed under N_2-flow rates of 40 and 60 mL min^{-1} for the balance and purge gases, respectively. For the thermal decomposition temperatures, the onset (T_{onset}) and derivative onset (T'_{onset}) temperatures were determined from the thermogravimetric (TG) and derivative TG curves, respectively. Note that the T'_{onset} values were considered to be the start of the decomposition temperatures, because T_{onset} values typically overestimate the thermal decomposition temperatures.[29]

FTIR Spectroscopy

IR spectroscopy was performed on a Bruker Vertex 80v IR spectrometer. We collected 128 and 512 scans for the background and sample measurements, respectively. The measurements were performed under vacuum within the range 4000–400 cm^{-1} at a resolution of 2 cm^{-1}. Samples of pristine MIL-53(Al) and the IL/MIL-53(Al)

composites were directly placed between two KBr windows, whilst the bulk ILs were mixed with KBr powder (>99%, Merck) prior to the measurements. IR bands were deconvoluted by using Fityk[34] software with the Voigt function.

Conductor-like Screening Model for Realistic Solvents (COSMO-RS) Calculations

We used the COSMOThermX software, version C30_1601 (COSMOlogic GmbH & Co. KG, Germany),[35] to predict the gas solubilities of the ILs at 25 °C within the pressure range 0.1–5 bar. TVZP parametrization was used for the calculations. The solubilities of CO_2, CH_4, and N_2 in the ILs were obtained from the activity coefficients.

High-Pressure Volumetric Adsorption (HPVA) Analysis

The gas-adsorption measurements of the pristine MOF and the IL/MOF composites were performed on a Micromeritics (Particulate Systems) HPVA II-200 high-pressure volumetric uptake analyzer.[36] Before each measurement, the sample was weighed and this value was recorded as the wet sample weight. Then, the sample was loaded into the sample holder and connected to the degas port of the equipment. Pristine MIL-53(Al) and all of the IL/MIL-53(Al) composites were activated at 150 °C under vacuum ($P = 10^{-6}$ bar) for 10 h. Once the degassing step was complete, the sample holder was placed in a water bath, which was connected to a circulator to maintain a constant temperature of 25 °C. Then, the sample holder was connected to the analysis port. To remove the residual gases, all of the lines were purged with helium three times just prior to the analysis. All of the measurements were performed within the pressure range 0.1–5 bar at 25 °C. When the measurements were complete, the sample was weighed and this value was recorded as the dry sample weight. This weight was used in the gas-adsorption calculations.

Acknowledgements

This study was supported by the Koç University Seed Fund Program and by the Scientific and Technological Research Council of Turkey (TUBITAK; Project No. 114R093). We are grateful for support from the Koç University TÜPRAŞ Energy Center (KUTEM) and Koç University Surface Science and Technology Center (KUYTAM). A.U. acknowledges a TUBA-GEBIP Award and TARLA for their support of this collaborative research. S.K. acknowledges ERC-2017-Starting Grant. This research has received funding from the European Research Council (ERC) under the European Union's Horizon 2020 research and innovation programme(ERC-2017-Starting Grant, grant agreement no. 756489-COSMOS).

Conflict of interest

The authors declare no conflict of interest.

Keywords: adsorption · CO_2 separation · gas separation · ionic liquids · metal–organic frameworks

[1] K. Sumida, D. L. Rogow, J. A. Mason, T. M. McDonald, E. D. Bloch, Z. R. Herm, T. H. Bae, J. R. Long, *Chem. Rev.* **2012**, *112*, 724–781.
[2] P. Nugent, E. G. Giannopoulou, S. D. Burd, O. Elemento, E. G. Giannopoulou, K. Forrest, T. Pham, S. Ma, B. Space, L. Wojtas, M. Eddaoudi, M. J. Zaworotko, *Nature* **2013**, *495*, 80–84.
[3] Y. S. Xue, W. Cheng, J. P. Cao, Y. Xu, *Chem. Asian J.* **2019**, *14*, 1949–1957.
[4] W. P. Lustig, S. Mukherjee, N. D. Rudd, A. V. Desai, J. Li, S. K. Ghosh, *Chem. Soc. Rev.* **2017**, *46*, 3242–3285.
[5] S. Keskin, S. Kızılel, *Ind. Eng. Chem. Res.* **2011**, *50*, 1799–1812.
[6] J. Y. Lee, C. Y. Tang, F. Huo, *Sci. Rep.* **2014**, *4*, 1–5.
[7] İ. Eruçar, G. Yılmaz, S. Keskin, *Chem. Asian J.* **2013**, *8*, 1692–1704.
[8] H. Li, K. Wang, Y. Sun, C. T. Lollar, J. Li, H. C. Zhou, *Mater. Today* **2018**, *21*, 108–121.
[9] S. Keskin, T. M. van Heest, D. S. Sholl, *ChemSusChem* **2010**, *3*, 879–891.
[10] B. Li, H. Wang, B. Chen, *Chem. Asian J.* **2014**, *9*, 1474–1498.
[11] K. K. Tanabe, S. M. Cohen, *Chem. Soc. Rev.* **2011**, *40*, 498–519.
[12] M. L. Foo, S. Horike, T. Fukushima, Y. Hijikata, Y. Kubota, M. Takata, S. Kitagawa, *Dalton Trans.* **2012**, *41*, 13791–13794.
[13] S. Parshamoni, S. Sanda, H. S. Jena, S. Konar, *Chem. Asian J.* **2015**, *10*, 653–660.
[14] L. Dai, S. Yu, Y. Shan, M. He, *Eur. J. Inorg. Chem.* **2004**, 237–241.
[15] M. Babucci, C. Y. Fang, A. S. Hoffman, S. R. Bare, B. C. Gates, A. Uzun, *ACS Catal.* **2017**, *7*, 6969–6972.
[16] R. K. Blundell, P. Licence, *Chem. Commun.* **2014**, *50*, 12080–12083.
[17] J. F. Brennecke, B. E. Gurkan, *J. Phys. Chem. Lett.* **2010**, *1*, 3459–3464.
[18] K. Fujie, H. Kitagawa, *Coord. Chem. Rev.* **2016**, *307*, 382–390.
[19] B. Zhang, J. Zhang, B. Han, *Chem. Asian J.* **2016**, *11*, 2610–2619.
[20] Y. Zhou, J. Qu, *ACS Appl. Mater. Interfaces* **2017**, *9*, 3209–3222.
[21] F. Wang, J. H. Jeon, S. J. Ki, J. O. Park, S. Park, *J. Mater. Chem. B* **2016**, *4*, 5015–5024.
[22] M. Díaz, A. Ortiz, I. Ortiz, *J. Membr. Sci.* **2014**, *469*, 379–396.
[23] J. P. Hallett, T. Welton, *Chem. Rev.* **2011**, *111*, 3508–3576.
[24] D. Chen, W. Ying, Y. Guo, Y. Ying, X. Peng, *ACS Appl. Mater. Interfaces* **2017**, *9*, 44251–44257.
[25] F. P. Kinik, A. Uzun, S. Keskin, *ChemSusChem* **2017**, *10*, 2842–2863.
[26] K. B. Sezginel, S. Keskin, A. Uzun, *Langmuir* **2016**, *32*, 1139–1147.
[27] V. Nozari, M. Zeeshan, S. Keskin, A. Uzun, *CrystEngComm* **2018**, *20*, 7137–7143.
[28] B. Koyuturk, C. Altintas, F. P. Kinik, S. Keskin, A. Uzun, *J. Phys. Chem. C* **2017**, *121*, 10370–10381.
[29] F. P. Kinik, C. Altintas, V. Balci, B. Koyuturk, A. Uzun, S. Keskin, *ACS Appl. Mater. Interfaces* **2016**, *8*, 30992–31005.
[30] M. Zeeshan, S. Keskin, A. Uzun, *Polyhedron* **2018**, *155*, 485–492.
[31] M. Mohamedali, H. Ibrahim, A. Henni, *Chem. Eng. J.* **2018**, *334*, 817–828.
[32] M. Zeeshan, V. Nozari, B. Yagci, T. Isik, U. Unal, V. Ortalan, S. Keskin, A. Uzun, *J. Am. Chem. Soc.* **2018**, *140*, 10113–10116.
[33] H. Kulak, H. M. Polat, S. Kavak, S. Keskin, A. Uzun, *Energy Technol.* **2019**, *7*, 1900157.
[34] M. Wojdyr, *J. Appl. Crystallogr.* **2010**, *43*, 1126–1128.
[35] COSMOtherm (COSMOlogic GmbH & Co. KG), http://www.cosmologic.de, accessed 30.05.2019.
[36] HPVA II–High Pressure Volumetric Analyzer (Particulate Systems, a division of Micromeritics), http://particulatesystems.com/hpva2/, accessed 14.11.2018.
[37] S. Bourrelly, P. L. Llewellyn, C. Serre, F. Millange, T. Loiseau, G. Ferey, *J. Am. Chem. Soc.* **2005**, *127*, 13519–13521.
[38] T. Loiseau, C. Serre, C. Huguenard, G. Fink, F. Taulelle, M. Henry, T. Bataille, G. Ferey, *Chem. Eur. J.* **2004**, *10*, 1373–1382.
[39] S. S. Y. Chui, S. M. F. Lo, J. P. H. Charmant, A. G. Orpen, I. D. Williams, *Science* **1999**, *283*, 1148–1150.
[40] S. Keskin, J. Liu, J. K. Johnson, D. S. Sholl, *Microporous Mesoporous Mater.* **2009**, *125*, 101–106.
[41] A. Vishnyakov, P. I. Ravikovitch, A. V. Neimark, M. Bülow, Q. M. Wang, *Nano Lett.* **2003**, *3*, 713–718.
[42] K. S. Park, Z. Ni, A. P. Côté, J. Y. Choi, R. Huang, F. J. Uribe-Romo, H. K. Chae, M. O'Keeffe, O. M. Yaghi, *Proc. Natl. Acad. Sci. USA* **2006**, *103*, 10186–10191.
[43] W. P. Mounfield III, K. S. Walton, *J. Colloid Interface Sci.* **2015**, *447*, 33–39.
[44] S. Cha, M. Ao, W. Sung, B. Moon, B. Ahlström, P. Johansson, Y. Ouchi, D. Kim, *Phys. Chem. Chem. Phys.* **2014**, *16*, 9591–9601.

[45] N. E. Heimer, R. E. Del Sesto, Z. Meng, J. S. Wilkes, W. R. Carper, *J. Mol. Liq.* **2006**, *124*, 84 – 95.
[46] S. A. Katsyuba, E. E. Zvereva, A. Vidiš, P. J. Dyson, *J. Phys. Chem. A* **2007**, *111*, 352 – 370.
[47] B. Schwenzer, S. N. Kerisit, M. Vijayakumar, *RSC Adv.* **2014**, *4*, 5457 – 5464.
[48] K. Nakamoto in *Infrared and Raman Spectra of Inorganic and Coordination Compounds*, 4th ed., Wiley, New York, NY, **1986**.
[49] A. Decken, A. Mailman, J. Passmore, J. M. Rautiainen, W. Scherer, E. W. Scheidt, *Dalton Trans.* **2011**, *40*, 868 – 879.
[50] A. Borba, A. Gómez-Zavaglia, P. N. N. L. Simões, R. Fausto, *Spectrochim. Acta Part A* **2005**, *61*, 1461 – 1470.
[51] K. Hanke, M. Kaufmann, G. Schwaab, M. Havenith, C. T. Wolke, O. Gorlova, M. A. Johnson, B. P. Kar, W. Sander, E. Sanchez-Garcia, *Phys. Chem. Chem. Phys.* **2015**, *17*, 8518 – 8529.
[52] S. Couck, J. F. M. Denayer, G. V. Baron, T. Rémy, J. Gascon, F. Kapteijn, *J. Am. Chem. Soc.* **2009**, *131*, 6326 – 6327.
[53] N. A. Ramsahye, G. Maurin, S. Bourrelly, P. L. Llewellyn, C. Serre, T. Loiseau, T. Devic, G. Férey, *J. Phys. Chem. C* **2008**, *112*, 514 – 520.
[54] S. Andonova, E. Ivanova, J. Yang, K. Hadjiivanov, *J. Phys. Chem. C* **2017**, *121*, 18665 – 18673.
[55] A. E. J. Hoffman, L. Vanduyfhuys, I. Nevjestic, J. Wieme, S. M. J. Rogge, H. Depauw, P. Van Der Voort, H. Vrielinck, V. Van Speybroeck, *J. Phys. Chem. C* **2018**, *122*, 2734 – 2746.
[56] K. M. Gupta, Y. Chen, Z. Hu, J. Jiang, *Phys. Chem. Chem. Phys.* **2012**, *14*, 5785 – 5794.
[57] K. M. Gupta, Y. Chen, J. Jiang, *J. Phys. Chem. C* **2013**, *117*, 5792 – 5799.
[58] Y. Chen, Z. Hu, K. M. Gupta, J. Jiang, *J. Phys. Chem. C* **2011**, *115*, 21736 – 21742.
[59] M. Fallanza, M. G. Miquel, E. Ruiz, A. Ortiz, D. Gorri, J. Palomar, *Chem. Eng. J.* **2013**, *220*, 284 – 293.
[60] X. Zhao, Q. Yang, D. Xu, Z. Bao, Y. Zhang, B. Su, Q. Ren, H. Xing, *AIChE J.* **2015**, *61*, 2016 – 2027.
[61] Y. Zhao, R. Gani, R. M. Afzal, X. Zhang, S. Zhang, *AIChE J.* **2017**, *63*, 1353 – 1367.
[62] M. Diedenhofen, A. Klamt, *Fluid Phase Equilib.* **2010**, *294*, 31 – 38.
[63] A. Jalal, E. Can, S. Keskin, R. Yildirim, A. Uzun, *J. Mol. Liq.* **2019**, *284*, 511 – 521.
[64] W. Xue, Z. Li, H. Huang, Q. Yang, D. Liu, Q. Xu, C. Zhong, *Chem. Eng. Sci.* **2016**, *140*, 1 – 9.
[65] F. Martínez, R. Sanz, G. Orcajo, D. Briones, V. Yángüez, *Chem. Eng. Sci.* **2016**, *142*, 55 – 61.
[66] B. H. Lim, W. H. Choe, J. J. Shim, C. S. Ra, D. Tuma, H. Lee, C. S. Lee, *Korean J. Chem. Eng.* **2009**, *26*, 1130 – 1136.
[67] B. Wang, H. Huang, X. L. Lv, Y. Xie, M. Li, J. R. Li, *Inorg. Chem.* **2014**, *53*, 9254 – 9259.
[68] S. Seth, G. Savitha, J. N. Moorthy, *Inorg. Chem.* **2015**, *54*, 6829 – 6835.
[69] A. Demessence, D. M. D'Alessandro, M. L. Foo, J. R. Long, *J. Am. Chem. Soc.* **2009**, *131*, 8784 – 8786.
[70] K. Sumida, S. Horike, S. S. Kaye, Z. R. Herm, W. L. Queen, C. M. Brown, F. Grandjean, G. J. Long, A. Dailly, J. R. Long, *Chem. Sci.* **2010**, *1*, 184 – 191.
[71] S. Galli, A. Maspero, C. Giacobbe, G. Palmisano, L. Nardo, A. Comotti, I. Bassanetti, P. Sozzani, N. Masciocchi, *J. Mater. Chem. A* **2014**, *2*, 12208 – 12221.
[72] Y. Xiong, Y. Z. Fan, R. Yang, S. Chen, M. Pan, J. J. Jiang, C. Y. Su, *Chem. Commun.* **2014**, *50*, 14631 – 14634.
[73] Q. Mu, H. Wang, L. Li, C. Wang, Y. Wang, X. Zhao, *Chem. Asian J.* **2015**, *10*, 1864 – 1869.
[74] C. Chen, J. Kim, D. A. Yang, W. S. Ahn, *Chem. Eng. J.* **2011**, *168*, 1134 – 1139.
[75] M. H. Choi, H. J. Park, D. H. Hong, M. P. Suh, *Chem. Eur. J.* **2013**, *19*, 17432 – 17438.
[76] M. Y. Masoomi, K. C. Stylianou, A. Morsali, P. Retailleau, D. Maspoch, *Cryst. Growth Des.* **2014**, *14*, 2092 – 2096.
[77] A. Phan, J. Doonan, F. J. Uribe-Romo, C. B. Knobler, M. O'Keeffe, O. M. Yaghi, *Acc. Chem. Res.* **2010**, *43*, 58 – 67.
[78] B. Wang, A. P. Côté, H. Furukawa, M. O'Keeffe, O. M. Yaghi, *Nature* **2008**, *453*, 207 – 212.

Manuscript received: May 13, 2019
Revised manuscript received: June 5, 2019
Version of record online: July 24, 2019

